Desalination and Water Treatment
www.deswater.com

doi: 10.1080/19443994.2015.1085449

57 (2016) 17512–17522
August

Taylor & Francis
Taylor & Francis Group

A comparative study of different diatomite-supported TiO_2 composites and their photocatalytic performance for dye degradation

Guangxin Zhang, Bin Wang, Zhiming Sun*, Shuilin Zheng*, Shushu Liu

School of Chemical and Environmental Engineering, China University of Mining and Technology (Beijing), Beijing 100083, P.R. China, emails: 136092842@qq.com (G. Zhang), 12339424@qq.com (B. Wang), Fax: +86 10 62339920; email: szmcumtb@hotmail.com (Z. Sun), Fax: +86 10 62331345; emails: shuilinzheng8@gmail.com (S. Zheng), 415484066@qq.com (S. Liu)

Received 25 January 2015; Accepted 14 August 2015

ABSTRACT

Three kinds of diatomites as catalyst carriers were adopted to prepare supported TiO_2 catalysts by a typical hydrolysis–deposition method. The prepared composites were characterized by X-ray diffraction, Fourier transform infrared spectroscopy, N_2 adsorption–desorption, scanning electron microscopy transmission electron microscopy, UV–vis diffuser reflectance, and chemical oxygen demand. The photocatalytic properties of composites were determined using rhodamine B, methyl orange, and methylene blue as target pollutants under UV light irradiation. A comparative study on the photocatalytic properties of composite catalysts was carried out. It is indicated that the catalytic performance of TiO_2/diatomite is significantly influenced by the physicochemical properties of diatomite supports. Compared with pure TiO_2, the TiO_2/diatomite composites exhibited smaller crystalline size of TiO_2 and better dispersibility, which induced higher specific surface area and better photo-degradation efficiency. The highest activity of the photocatalyst should be attributed to the acid-activated support, which provided more active sites for the degradation reaction. Besides, the durabilities of catalysts were also investigated. The experimental results indicated that the prepared composite is a promising material for the wastewater treatment for its good photocatalytic property and reusability.

Keywords: Support; Diatomite; TiO_2; Dye; Photocatalysis

1. Introduction

Due to the fast development of textile industry, a large amount of dye wastewater has been released into the environment without treatment, which can lead to significant environmental problems. Many nitrogenous dyes, such as azo dyes, can yield potentially carcinogenic aromatic amines which undergo natural degradation [1–3]. Many researchers have reported the feasibility of using various semiconductor photocatalysts for the treatment of textile wastewater because of their good removal effect and low energy cost [4–6]. Titanium dioxide (TiO_2) has been extensively used in the air purification, wastewater treatment, and other environmental fields due to its good biological and chemical inertness, nontoxic, and relatively low cost [7–10]. As a photocatalyst, however, traditional TiO_2 powder has some disadvantages because of their low adsorption capacity, poor

*Corresponding authors.

reusability, and difficult separation from aqueous solution [11].

In recent years, different immobilization techniques to prepare supported TiO_2 composites appear to provide some feasible solutions to such problems [12,13]. A number of different materials were used for supporting TiO_2 such as zeolite [14], cenosphere [15], carbon [16], and glass slide [17]. The natural non-metallic mineral materials have porous microstructure, large specific surface area, high chemical and thermal stabilities, good ion exchange, and adsorption capacity, which are favorable to act as catalyst support. Immobilizing the nano-TiO_2 particles on porous non-metallic minerals is not only beneficial to improve the efficiency of photocatalysis but also favors the separation and recovery of catalysts from aqueous solution. In the last few years, some natural minerals, such as sepiolite [18], montmorillonite [19], diatomite [20], kaolin [21], and attapulgite [22], have been reported to be used as the carriers of the composite photocatalysts. Among various porous natural minerals, diatomite seems to be an attractive candidate due to its porous structure, high adsorption capacity, low cost, and large reserves [23–25]. Diatomite is a kind of biogenic silica sedimentary rock, formed from the deposition of single-celled aquatic algae, consisting of a significant number of diatom units with various shapes and sizes. TiO_2 loaded on diatomite can significantly increase the specific surface area and adsorption performance, offering more active sites for the degradation of pollutants [26]. The pretreatment of diatomite can influence the photocatalysis of composites such as acid leaching of the diatomite. Liu et al. [27] discussed the effect of diatomite which was treated with the H_2SO_4/HF-mixed acid solution and calcined at 1,000˚C on the catalytic performance of titanium silicalite/diatomite. Xia et al. [28] prepared TiO_2 diatomite by sol–gel method with various pre-modified diatomites and confirmed the effects of carrier on the structure and properties of supported TiO_2. However, to the best of our knowledge, these experiments merely treated one pollutant, which may not be representative, and the catalytic performance may be different to diverse pretreatments. The research for the treatment of dyeing wastewater by nano-TiO_2/diatomite composites has an important significance obviously.

In this work, it synthesized three kinds of TiO_2/diatomite composites using different pretreated supports by a typical hydrolysis–deposition method. The photocatalytic properties of the composites were determined by the degradation of rhodamine B, methyl orange, and methylene blue under UV light irradiation. The crystalline size of TiO_2, surface area, surface potential, and other properties related to the adsorption/photocatalysis capability of catalysts were also studied in order to investigate the effect of different pretreated diatomites on the photocatalysis of the obtained products.

2. Experimental

2.1. Materials

Calcined diatomite (CD) was provided by Xinghui Filtering Aid Ltd (Jilin province, China). Diatomite that was provided by Beifeng Diatomite Ltd (Jilin province, China) was treated by physical purification according to the literature [25] and labeled as PD. PD was calcined at 500˚C for 1 h and pretreated with 50 wt.% sulfuric acid subsequently; the acid-purified diatomite was labeled as APD. The main chemical compositions of CD, PD, and APD are listed in Table 1. Titanium tetrachloride ($TiCl_4$), sulfuric acid (H_2SO_4), hydrochloric acid (HCl), ammonium sulfate [$(NH_4)_2SO_4$], and ammonia liquor ($NH_3{\cdot}H_2O$) were purchased from Beijing Chemical Works. Rhodamine B ($C_{28}H_{31}ClN_2O_3$, RB), methyl orange ($C_{14}H_{12}N_3O_3$-NaS, MO), and methylene blue ($C_{16}H_{18}ClN_3S$, MB) used as model contaminants were purchased from Aladdin Chemistry Co. Ltd. All agents were used without further purification. Degussa P-25 (Germany) was used as a reference material. Deionized water was used throughout the experiment.

2.2. Preparation of TiO_2/diatomite catalysts

The preparation of TiO_2/diatomite composite was undertaken by a typical hydrolysis–deposition method using $TiCl_4$ as a precursor. Initially, the diatomite powders were added to a flask containing a certain amount of deionized water, which was kept in a ice-water bath under vigorous stirring. Then, $TiCl_4$ solution and $(NH_4)_2SO_4$ solution were added to the suspension at an interval of 15 min according to the 1:1 (molar ratio) of $[Ti^{4+}]/[SO_4^{2-}]$ at a preset dropping rate. The theoretical loading amount of TiO_2 was determined as 40 wt.% (TiO_2: diatomite = 2:5), which was controlled by the adding a certain amount of $TiCl_4$ solution. After stirring for another 15 min, the temperature was increased to 40˚C followed by successive stirring for 1 h. The final pH value of the dispersion was adjusted to about 5.5 through the addition of diluted ammonia solution. After 1 h, the suspension was filtrated by a vacuum filter and washed free of chloride anions as determined by the use of 0.1 M $AgNO_3$ solution. The product was dried in an oven at 105˚C for 8 h with subsequent calcination at

Table 1
Chemical constituents (wt.%) and surface area of diatomite

Sample	SiO_2	Al_2O_3	Fe_2O_3	MgO	TiO_2	LOI[a]	BET surface area (m^2/g)
CD	92.03	2.38	1.32	0.29	0.11	0.33	1.83
PD	86.52	4.05	2.25	0.39	0.22	4.18	15.58
APD	92.27	2.21	0.48	0.56	0.21	2.84	26.20

[a]Loss on ignition.

700 ℃ for 2 h in the air at a heating rate of 2.5 ℃/min. The three prepared samples using different diatomites were denoted as T-CD, T-PD, and T-APD, respectively. Pure TiO_2 without diatomite as reference was also synthesized, which was denoted as PT.

2.3. Characterization of catalysts

The phases of samples were characterized by X-ray powder diffraction (XRD) analysis on D8-ADVANCE X-ray power diffractometer (Bruker, Germany) with Cu–Kα radiation (λ = 0.15406 nm) under the operation conditions of 40 kV and 40 mA. The samples were scanned at a rate of 4˚/min. FT-IR spectra of the samples mixed with KBr were obtained using Fourier transform infrared spectrometer (Nicolet iS10, USA). The surface area of samples was measured by N_2 adsorption at 77 K on a constant volume adsorption apparatus (JW-BK, JWGB Science and Technology, China) and calculated by the Brunaer–Emmett–Teller (BET) method. The surface morphologies and microstructures were observed by S-4800 scanning electron microscopy (Hitachi, Japan) and transmission electron microscopy (TEM, JEM 1200EX, JEOL Ltd). The isoelectric point of the samples was tested by Zeta-potential instrument (Nano ZS90, UK). The optical properties of the samples were characterized by UV–vis diffuse reflectance spectroscopy (DRS) using a UV–vis spectrophotometer (UV-9000S, Shanghai Metash, China) equipped with diffusive reflectance accessory. Chemical oxygen demand (COD) measurements were carried out by the dichromate titration method on the RB solutions under UV light irradiation.

2.4. Adsorption/photocatalysis of catalysts

The photocatalytic activity of catalysts was evaluated by the degradation of dyes (RB, MO, and MB) in aqueous solution under 300-W high-pressure mercury lamp (λ_{max} = 365 nm) as UV light. Experiments were conducted in a photocatalytic reactor (Shanghai Bilon Instruments Corporate, China) [10]. The quartz tube (150 mL) was positioned at a fixed distance of 10 cm from the lamp. The solution was stirred mechanically in the tube at a constant rate using a magnetic stirrer during the reaction. The lamp was positioned inside the double-deck quartz cold trap through which circulating water was used to cool the lamp. For the degradation of dye, 0.1 g of prepared catalyst was added into 100 mL dyes (10 mg/L). Prior to UV illumination, the suspension was stirred vigorously for 30 min or 1 h in the dark to establish the adsorption–desorption equilibrium between the dye and catalyst. The suspension was withdrawn from the reactor at set intervals and centrifuged. The photocatalytic discoloration of the dye was analyzed by UV–vis spectrophotometer (UV-9000S, Shanghai Metash, China) through measuring the absorbance change at 464 nm (MO), 554 nm (RB), and 664 nm (MB). The percentage of dye degradation (D) was calculated by the following equation:

$$D = \frac{C_0 - C_t}{C_0} \times 100\% \quad (1)$$

where C_0 and C_t are the concentrations of dye at initial time and at time t, respectively.

3. Results and discussion

3.1. XRD analysis

The XRD patterns of the obtained TiO_2/diatomite composites and pure TiO_2 powder are shown in Fig. 1. In the pattern of T-CD, there are three representative peaks around 2θ = 21.9˚, 31.3˚, and 36.0˚, which could be ascribed to the cristobalite (No. 39-1425). The phase transformation came from the amorphous opal calcined above 1,100 ℃. T-PD and T-APD composites have a very wide asymmetric diffraction peak at 2θ between 18˚ and 28˚, which is consistent with the diffraction peaks of the amorphous SiO_2. There is a characteristic diffraction peak at 2θ = 26.7˚ corresponding to quartz in T-PD and T-APD [29]. T-CD, T-PD, and T-APD have weak quartz

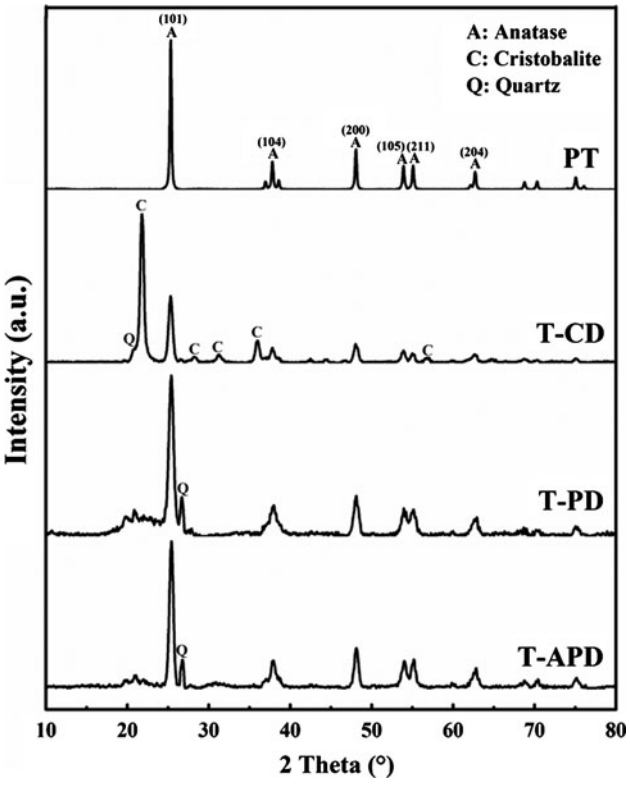

Fig. 1. XRD patterns of various composite catalysts and pure TiO_2.

diffraction peaks. The XRD patterns of TiO_2 particles show the presence of three main peaks at $2\theta = 25.3^\circ$ (1 0 1), 37.8° (0 0 4), and 48.1° (2 0 0), which are representatives of anatase TiO_2. According to Fig. 1, no evident peaks of rutile-TiO_2 phases appear in the XRD patterns of pure TiO_2, which is because that SO_4^{2-} (originated from adding $(NH_4)_2SO_4$ during the preparation process) retarded the phase transition from anatase to rutile [30].

The crystalline size of TiO_2 in the samples was calculated by the Scherrer equations:

$$D = K\lambda/\beta\cos\theta \quad (2)$$

where D was the crystalline size, λ was the X-ray wavelength (0.15406 nm), β was the full width at half maximum of the (1 0 1) peak, θ was the half angle of the diffraction peak, and $K = 0.89$. By calculating, the crystalline sizes of TiO_2 in three catalysts are around 13–15 nm, which indicates that the difference between supports has no influence on the particle size of supported TiO_2. The crystalline size of pure TiO_2 (33 nm) was larger than that of supported TiO_2, which means diatomite as the support can inhibit the growth of TiO_2 grains [11]. This is because diatomite dispersed TiO_2 particles and impeded the agglomeration of it.

3.2. Morphology analysis

The SEM and TEM images of three kinds of diatomites, TiO_2/diatomite catalysts, and PT are displayed in Fig. 2. The microstructure of the CD, PD, and APD samples is exhibited in Fig. 2(a)–(c), respectively. In Fig. 2(a)–(c), the diatomite is mainly consisted of disc-like diatoms with a diameter of ca. 20–30 μm and has numerous ordered micropores on the surface. The CD has a smoother surface and larger pores than the other two kinds of diatomites. However, some micropores of CD are destroyed due to the high-temperature calcination. It is observed that some of the pores are blocked by impurities (clay minerals and organic matter) on the diatom of PD (Fig. 2(b)). The pores on the diatom of APD could be seen more clearly after acid leaching and calcination treatment (Fig. 2(c)). Compared with the unloaded diatomite, the surface of the TiO_2/diatomite composite becomes rougher because of the presence of TiO_2 particles. Moreover, the EDS measurement confirmed the composition of the hybrids (inset of Fig. 2(f)), which demonstrated the presence of Si, Ti, and O. According to the TEM images of PT (Fig. 2(i)), the TiO_2 nanoparticles have an average size of around 40 nm and dramatically congregate together, which is in line with the XRD result. From the TEM images of T-APD (Fig. 2(g) and (h)), it can be seen directly that the TiO_2 particles are uniformly distributed on the surface or in the pores of the diatomite, and the porous structure of diatomite is well preserved. It indicates that the diatomite as the support plays an important role on the dispersion of nano-TiO_2 particles. It has been reported that the particle size of photocatalyst is a crucial factor in the dynamics of the electron/hole recombination process [31]. In general, catalysts with smaller particle size would be favorable for higher catalytic activity.

3.3. FT-IR spectral analysis

The FT-IR spectra of TiO_2/diatomite catalysts are shown in Fig. 3. The samples exhibited characteristic peaks at 3,440 and 1,630 cm^{-1}, which can be assigned to the stretching vibration of O–H and bending vibrations of O–H bond of the physisorbed water, respectively [26,32]. These were derived from the surface of –OH groups of diatomite and TiO_2. More hydroxyl groups existing on the surface of catalysts favor the enhancement of the photocatalytic performance [33].

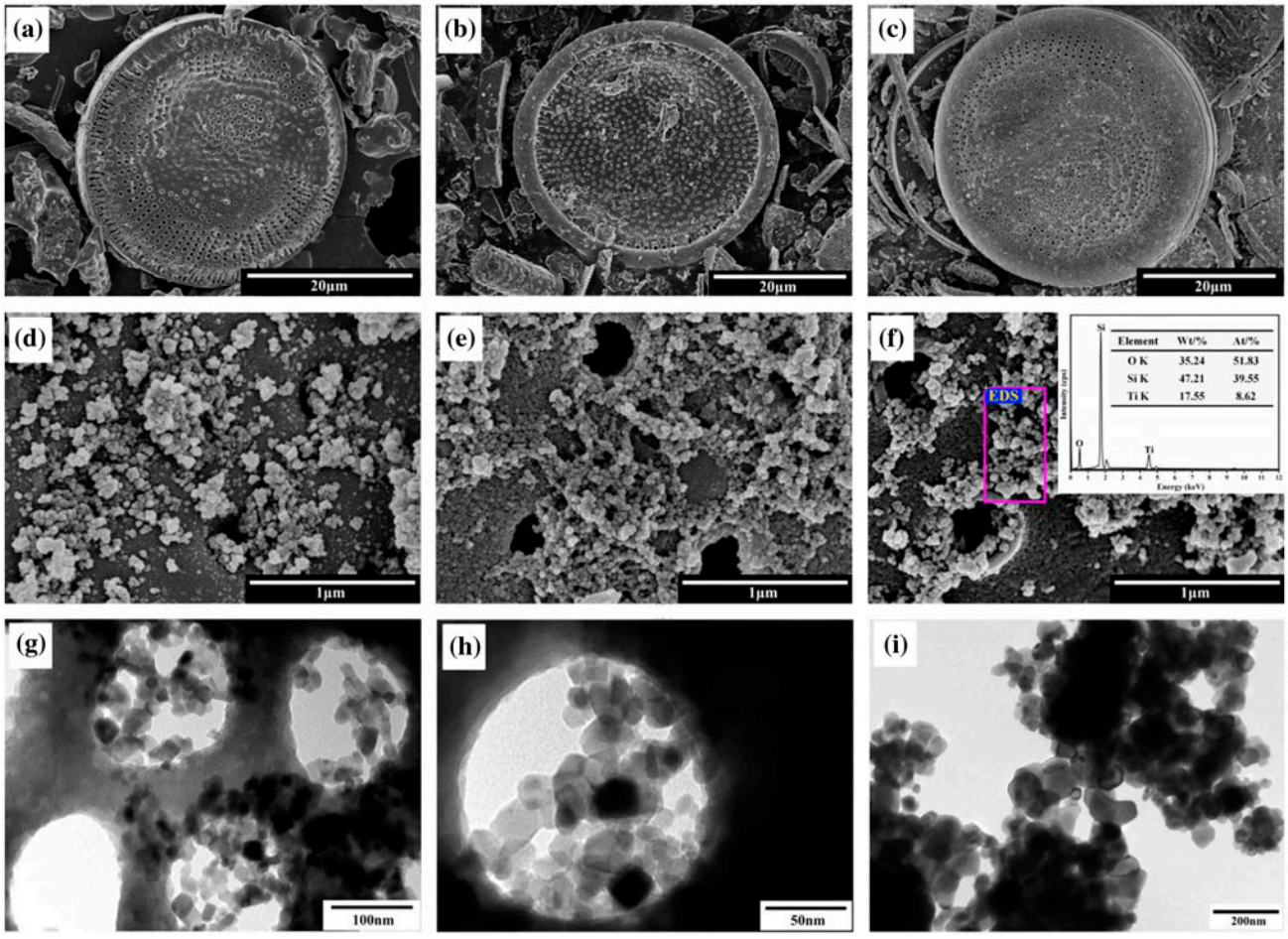

Fig. 2. SEM micrographs of (a) CD, (b) PD, (c) APD, (d) T-CD, (e) T-PD, and (f) T-APD (inset illustrates EDS results of T-APD), and TEM images of T-APD (g-h) and PT (i).

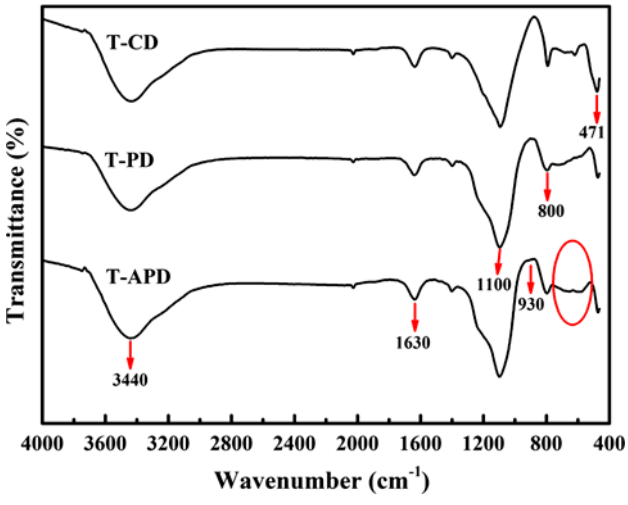

Fig. 3. FT-IR spectroscopy of TiO_2/diatomite composites.

The peaks located at 1,100, 800, and 471 cm^{-1} can be assigned to the asymmetric and symmetric stretching vibrations and bending vibrations of Si–O–Si. The wide band around 800–500 cm^{-1} corresponds to the characteristic absorption of TiO_2 [34]. The weak absorption peak at 930 cm^{-1}could have resulted from Si–O–Ti linkages [35], which were very weak at the spectra of prepared catalysts, probably due to the small number of these bonds.

3.4. DRS analysis

To investigate the optical absorption properties of TiO_2/diatomite composites, diffuse reflectance spectra (DRS) was analyzed (Fig. 4). The band gap energy was obtained corresponding to the intersection point of the vertical and horizontal parts, which was calculated according to the equation:

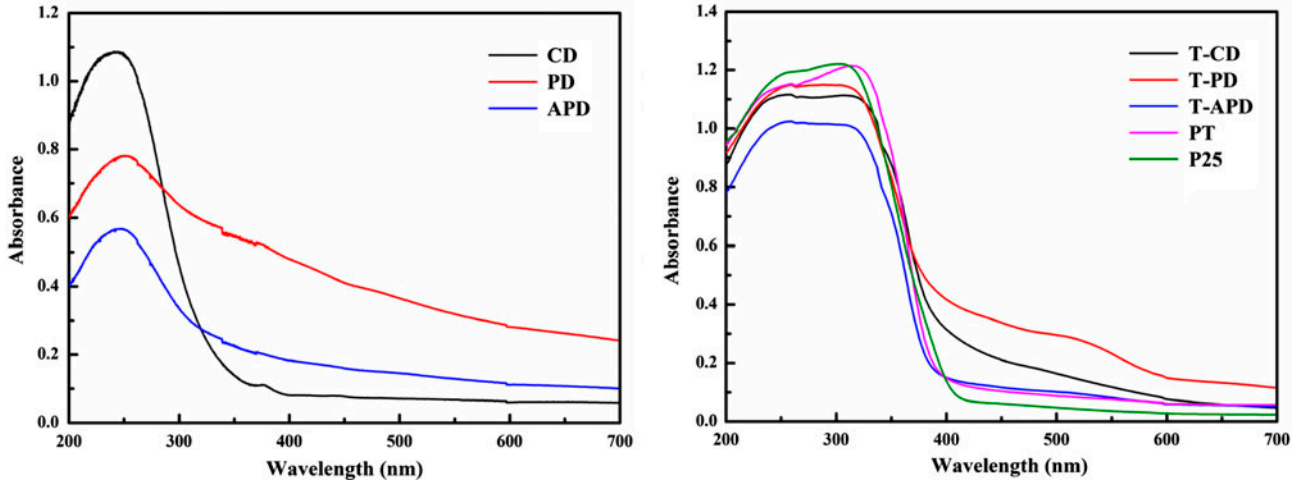

Fig. 4. UV–vis DRS spectra of diatomite, various composite catalysts, pure TiO_2, and P25.

$$E_g(\text{eV}) = 1{,}240/\lambda \quad (3)$$

where E_g is the band gap (eV) and λ (nm) is the wavelength of the absorption edges in the spectrum [36]. As shown in Fig. 4, the absorption edges of samples have no obvious difference, which indicates that these catalysts have the similar band gap. The obtained band gap energies are shown in Table 2. The band gap energies of the PT (3.18 eV) are higher than those of P25 (3.03 eV). This phenomenon can be ascribed to the quantum size effect of the TiO_2 particles. Meanwhile, the diatomite support could act as a photosensitizer and effectively extend the absorption into the visible light region [37]. The color of the prepared TiO_2/diatomite is different from each other. The color of T-PD is brown. T-CD exhibited a pale yellow color, while the color of T-APD is white. This phenomenon is related to the oxidation of the residual organic groups in the diatomite [38]. This result demonstrates that diatomite is not obviously effective for changing the band gap of TiO_2/diatomite and the DRS of TiO_2/diatomite was susceptible to diatomite.

3.5. Adsorption and photocatalytic performance of catalysts

Generally, photocatalysts with higher specific surface area would be favorable to higher catalytic activity [39]. The surface charge of catalysts may also influence the adsorption process. In this study, the adsorption of dyes on catalysts was carried out in dark for 30 min (or 1 h) to realize the adsorption–desorption equilibrium. The adsorption of dyes on catalysts was relatively rapid within 2 min and then slowed down before reaching the reaction equilibrium. For MO solutions, the adsorption capacities of PT and P25 were better than those of T-CD, T-PD, and T-APD. It is because MO is an anionic dye, and pH of the MO solution is 5.89, which is less than the isoelectric point of P25 (pH_{IEp} 6.8) [40]. So, the surface of PT and P25 particles is electropositive, resulting in a better adsorption capacity for MO dye, while the surfaces of three TiO_2/diatomite catalysts are electronegative (pH_{IEP}(T-PD) = 2.65, pH_{IEP}(T-CD) = 3.58, and pH_{IEP}(T-APD) = 3.33), which lead to lower adsorption. However, RB and MB are cationic dyes, and the pH of RB (4.87) and MB (5.62) solutions is

Table 2
Physical properties and kinetic constants for MB adsorption of catalysts

Sample	Crystalline size of anatase (nm)	Isoelectric point	BET surface area (m^2/g)	Band gap E_g (eV)	k (g/mg min)	q_e (mg/g)	R^2
T-CD	15	3.58	15.47	3.09	0.88	1.55	0.9993
T-PD	13	2.65	31.39	3.13	0.27	4.03	0.9997
T-APD	15	3.33	30.80	3.17	0.23	3.65	0.9993
PT	33	6.0	24.68	3.18	19.55	1.13	0.9999
P25	21	6.8	56.44	3.03	0.45	2.16	0.9998

greater than the isoelectric point of the three composite catalysts. The surfaces of three composite catalysts are electronegative, so they may adsorb RB and MB dyes easily. The larger surface area of T-PD and T-APD also has a contribution to the higher adsorption capacity (Table 2). Besides, the $\equiv SiO^-$ groups on the diatomite surface can combine with R-$N(CH_3)_2^+$ of MB and R-$N(C_2H_5)_2^+$ of RB. But, it also can be seen that P25 has a small amount of adsorption for MB and RB solutions; this may be due to the adsorption of MB (or RB) on TiO_2 through the nitrogen atoms that hydrogen bond to the surface hydroxyl groups [41].

In order to understand the mechanism of the adsorption process, the pseudo-second-order model was used to describe the adsorption kinetic [42]:

$$\frac{t}{q_t} = \frac{1}{kq_e^2} + \frac{1}{q_e}t \tag{4}$$

where k is the rate constant (g/mg min^{-1}) and q_t and q_e are the amounts of dye (mg/g) adsorbed at any time and at equilibrium, respectively. The kinetic curves and the kinetic constants of the adsorption of MB on various catalysts are shown in Fig. 5 and Table 2. The results indicated that the pseudo-second-order equation fitted well with the experiment data and could be used to describe the adsorption kinetics of TiO_2/diatomite.

The photocatalytic activities of catalysts were evaluated by decomposing the different dyes (MO, RB, MB, and MB + RB) in aqueous solutions under UV light irradiation. The dyes' degradation curves as a function of reaction time for catalysts are shown in Fig. 6. The blank tests of dyes without catalysts were also conducted as references. In addition, PT and P25 were also carried out for comparison. After turning on the lamp, the removal rate of MB without catalysts is very low (1.72% after 1 h irradiation). In the photocatalytic process, the adsorbed dye molecules were decomposed and simultaneously kept adsorbing on the catalysts' surface. After 1 h irradiation, the degradation efficiency of T-APD was up to 97.75%, which was a little more than that of P25. Within the same time interval, the degradation efficiencies of T-CD, T-PD, and PT were 93.99, 53.33, and 71.26%, respectively. For MB, the degradation capacity of different obtained catalysts can be summarized as follows: T-APD > P25 > T-CD > PT > T-PD.

Generally, the photocatalytic degradation can be well described by the Langmuir–Hinshelwood (L–H) kinetic model. This equation can be simplified to a pseudo-first-order equation as follows:

$$\ln\frac{C_0}{C_t} = kt \tag{5}$$

where k is the apparent rate constant and C_0 and C_t are the concentrations of dyes after adsorption/desorption equilibrium and at the time t [6]. The kinetic parameters are calculated and summarized in Table 3. The straight line functions with a high value of R^2 were obtained (not listed here), which indicated that the pseudo-first-order equation fitted well with the experimental data. T-APD has the highest k value for three dyes' degradation among the composite catalysts. For RB (Fig. 6(b)), the degradation behaviors of

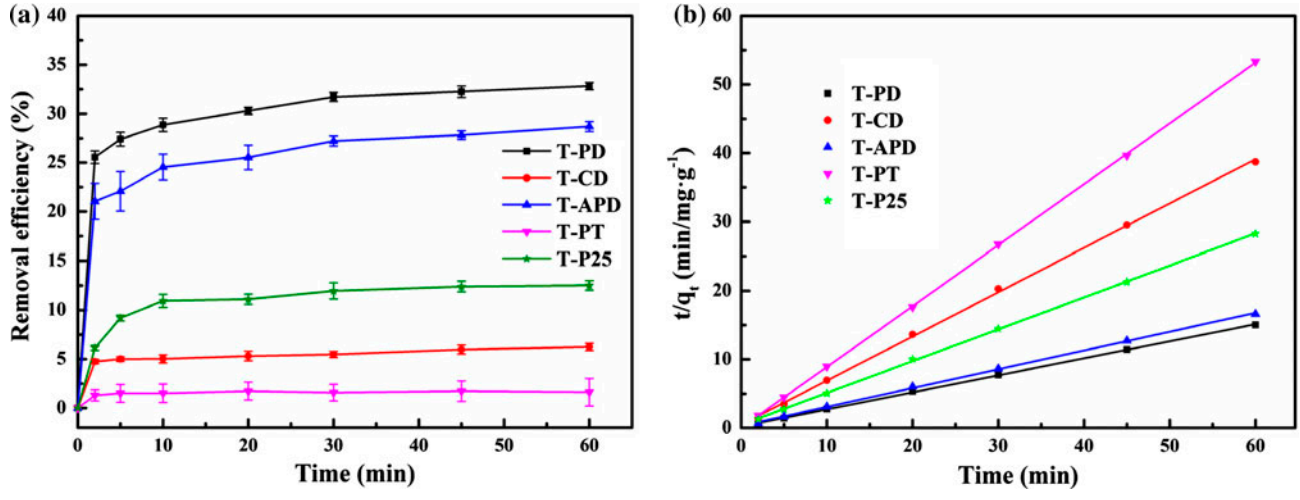

Fig. 5. Adsorption curve (a) and kinetic curves and (b) of the adsorption of MB on catalysts.

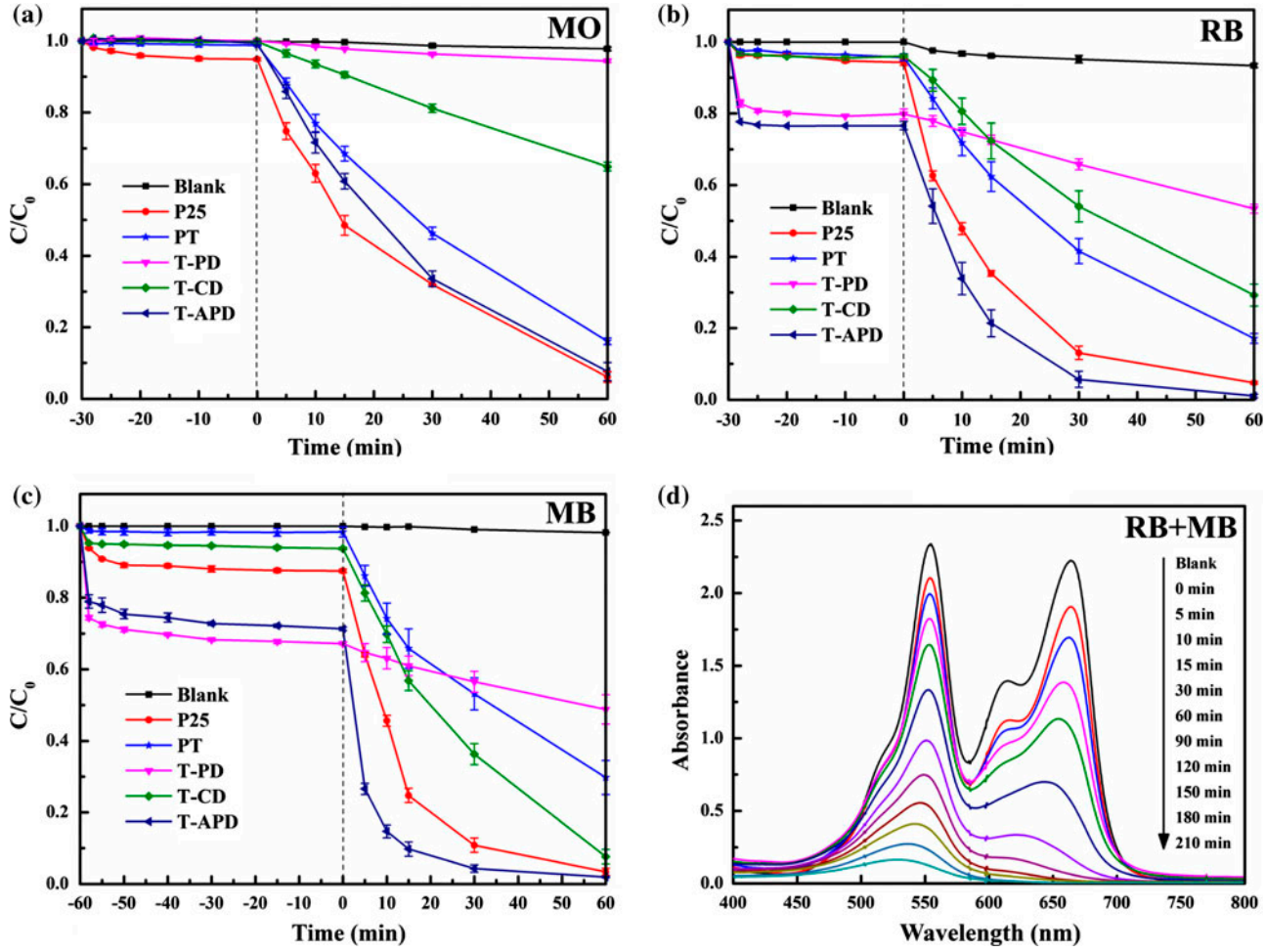

Fig. 6. The degradation of MO (a), RB (b), MB (c), and MB + RB (d) using different catalysts under UV light irradiation.

Table 3
Characteristics of dyes and the kinetic parameters of degradation of catalysts

Dye	Classification	λ_{max} (nm)	pH	Catalysts	k (min^{-1})	R^2
MO	Anionic	464	5.89	T-PD	0.001	0.9836
				T-CD	0.007	0.9992
				T-APD	0.041	0.9915
RB	Cationic	554	4.87	T-PD	0.007	0.9989
				T-CD	0.020	0.9990
				T-APD	0.075	0.9909
MB	Cationic	664	5.62	T-PD	0.006	0.9955
				T-CD	0.039	0.9847
				T-APD	0.102	0.9807
RB + MB	RB			T-APD	0.012	0.9964
	MB			T-APD	0.035	0.9898

catalysts are similar to those of MB. However, for MO (Fig. 6(a)), P25 is the best catalyst, which may be due to the fact that MO is an anionic dye. It would be more easy for PT to adsorb MO, which results in a better photocatalytic performance.

As summarized in Table 3, T-APD had the best photocatalytic performance, which could be attributed to the acid activation. Acid leaching removed the impurities within the diatomite effectively, which reduced the Lewis acid sites (resulted from the clay impurities) and increased the Brønsted acid sites [24,43]. Therefore, acid leaching modified the surface properties of the diatomite, which provided more active sites for the degradation reaction [44]. Because of the small surface area, T-CD didn't have a good adsorption capacity, which resulted in the lower photocatalytic capacity. Although T-PD possessed larger surface areas, its degradation rate was lower than the other catalysts. A few immobilized TiO_2 particles could not be activated by UV light irradiation because of the shielding effect of the impurities in PD. The photocatalytic activity toward mixed dyes (10 mg/L MB and 10 mg/L RB) was conducted using T-APD as a catalyst. The results are displayed in the Fig. 6(d). It was found that the photocatalytic degradation also follows the pseudo-first-order kinetics in the case of mixed dyes. The kinetic parameters are calculated and listed in Table 3. The data showed that the degradation rate of individual dyes in mixture was lower than that of single dye, which should be associated with the competition of dyes in mixtures to access the active centers of the composite catalyst [45].

To confirm the mineralization, the photocatalytic degradation reactions were carried out up to 90 min. The COD values of the RB solutions under UV irradiation over T-APD were measured and the results are represented in Fig. 7. Before turning on the light, the initial COD concentration of the RB solution is 17.75 mg/L. After 90 min of UV irradiation, the COD concentration of the RB solution decreases from 84.62% to 2.73 mg/L. The corresponding decolorization efficiencies were higher than those of COD removal efficiencies, which were probably due to the complete destruction of the chromophore of RB; but the organic pollutant has been oxidized to micromolecule pollutants, which have not been oxidized to CO_2 and H_2O [46]. The significant decrease in the COD values indicates the efficiency of the photocatalytic degradation methods for wastewater treatment [47].

Reusability is another important indicator for the practical application of environmental catalyst materials, except for catalytic performance. The reusability of the T-APD was studied by recycled

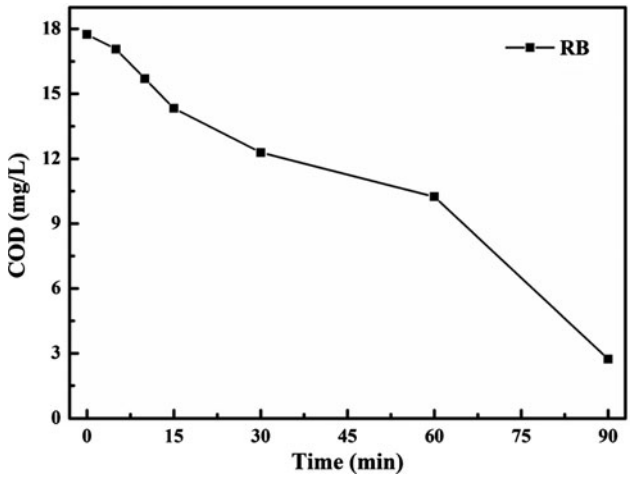

Fig. 7. COD data for the RB solutions under UV irradiation over T-APD.

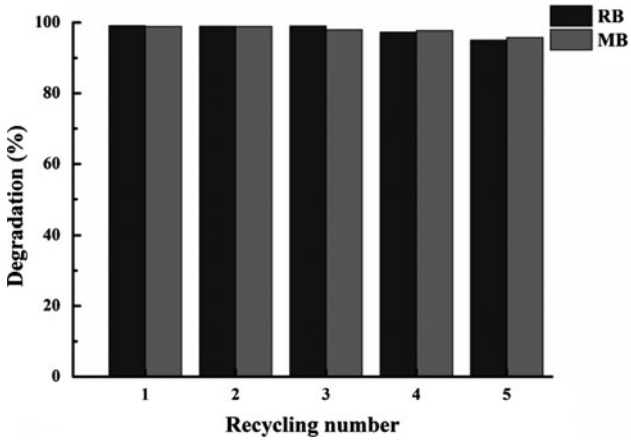

Fig. 8. Reusability of T-APD catalyst for dyes' degradation.

experiments under the same condition as described above, and the results are shown in Fig. 8. At the end of each cycle, the catalyst was reclaimed by filtration and washed with ethanol continuously, and then calcined at 500 °C for 30 min. After the fifth use, the removal efficiency of RB and MB was still above 95%. The observation revealed that the prepared composite did not exhibit significant loss of photocatalytic activity after five recycles, which indicated that the obtained composite possesses good reusability.

4. Conclusions

In this paper, TiO_2 particles were successfully loaded on three kinds of diatomites via hydrolysis of $TiCl_4$ followed by calcination. The support diatomite

can restrain the growth of the TiO_2 grains. SEM and TEM images indicate that TiO_2 particles are uniformly dispersed on the surface of the diatomite. Acid leaching and calcination treatments can improve the surface property of the diatom, so that the TiO_2 particles can combine with the diatomite firmly through the interaction force. The adsorption capacity of composite catalysts in dark condition was dependent on the surface charge and groups and specific surface area. The pseudo-second-order model can be used to describe the adsorption kinetics of MB on catalysts. The trend of photocatalytic activity for the three composite catalysts is summarized as follows: T-APD > T-CD > T-PD. The T-APD catalyst possesses the optimum photocatalytic performance for degrading methyl orange, rhodamine B, and methylene blue. The degradation efficiencies of dyes in the presence of the composite catalysts were found to follow the L–H kinetic model. Higher purity of the diatomite and relatively larger specific surface areas could be responsible for the higher photocatalytic activity of the T-APD sample. It is indicated that T-APD could be a promising catalyst for the sewage treatment, owing to its good photocatalytic property and reusability.

Acknowledgments

The authors gratefully acknowledge the financial support by the National Technology R&D Program in the 12th five years plan of China (Grant Number 2011BAB03B07).

References

[1] S. Wang, Z. Zhu, Effects of acidic treatment of activated carbons on dye adsorption, Dyes Pigm. 75 (2007) 306–314.
[2] T.A. Khan, S. Dahiya, I. Ali, Use of kaolinite as adsorbent: Equilibrium, dynamics and thermodynamic studies on the adsorption of Rhodamine B from aqueous solution, Appl. Clay Sci. 69 (2012) 58–66.
[3] H. Fu, C. Pan, W. Yao, Y. Zhu, Visible-light-induced degradation of rhodamine B by nanosized Bi_2WO_6, J. Phys. Chem. B 109 (2005) 22432–22439.
[4] R. Kralchevska, M. Milanova, M. Tsvetkov, D. Dimitrov, D. Todorovsky, Influence of gamma-irradiation on the photocatalytic activity of Degussa P25 TiO_2, J. Mater. Sci. 47 (2012) 4936–4945.
[5] M.A. Nawi, S.M. Zain, Enhancing the surface properties of the immobilized Degussa P-25 TiO_2 for the efficient photocatalytic removal of methylene blue from aqueous solution, Appl. Surf. Sci. 258 (2012) 6148–6157.
[6] Z. Sun, Z. Hu, Y. Yan, S. Zheng, Effect of preparation conditions on the characteristics and photocatalytic activity of TiO_2/purified diatomite composite photocatalysts, Appl. Surf. Sci. 314 (2014) 251–259.
[7] M.R. Hoffmann, S.T. Martin, W. Choi, D.W. Bahnemann, Environmental applications of semiconductor photocatalysis, Chem. Rev. 95 (1995) 69–96.
[8] A. Fujishima, T.N. Rao, D.A. Tryk, Titanium dioxide photocatalysis, J. Photochem. Photobiol., C: Photochem. Rev. 1 (2000) 1–21.
[9] X. Yang, C. Cao, L. Erickson, K. Hohn, R. Maghirang, K. Klabunde, Photo-catalytic degradation of Rhodamine B on C-, S-, N-, and Fe-doped TiO_2 under visible-light irradiation, Appl. Catal. B: Environ. 91 (2009) 657–662.
[10] Q. Sun, H. Li, S. Zheng, Z. Sun, Characterizations of nano-TiO_2/diatomite composites and their photocatalytic reduction of aqueous Cr(VI), Appl. Surf. Sci. 311 (2014) 369–376.
[11] B. Wang, G. Zhang, Z. Sun, S. Zheng, Synthesis of natural porous minerals supported TiO_2 nanoparticles and their photocatalytic performance towards Rhodamine B degradation, Powder Technol. 262 (2014) 1–8.
[12] T. Kamegawa, R. Kido, D. Yamahana, H. Yamashita, Design of TiO_2-zeolite composites with enhanced photocatalytic performances under irradiation of UV and visible light, Microporous Mesoporous Mater. 165 (2013) 142–147.
[13] M. Huang, C. Xu, Z. Wu, Y. Huang, J. Lin, J. Wu, Photocatalytic discolorization of methyl orange solution by Pt modified TiO_2 loaded on natural zeolite, Dyes Pigm. 77 (2008) 327–334.
[14] R.J. Tayade, R.G. Kulkarni, R.V. Jasra, Enhanced photocatalytic activity of TiO_2-coated NaY and HY zeolites for the degradation of methylene blue in water, Ind. Eng. Chem. Res. 46 (2007) 369–376.
[15] P.K. Surolia, R.J. Tayade, R.V. Jasra, TiO_2-coated cenospheres as catalysts for photocatalytic degradation of methylene blue, p-nitroaniline, n-decane, and n-tridecane under solar irradiation, Ind. Eng. Chem. Res. 49 (2010) 8908–8919.
[16] W. Jo, Y. Won, I. Hwang, R.J. Tayade, Enhanced photocatalytic degradation of aqueous nitrobenzene using graphitic carbon-TiO_2 composites, Ind. Eng. Chem. Res. 53 (2014) 3455–3461.
[17] R. Djellabi, M.F. Ghorab, Solar photocatalytic decolourization of crystal violet using supported TiO_2: Effect of some parameters and comparative efficiency, Desalin. Water Treat. 53 (2015) 3649–3655.
[18] Y. Zhang, D. Wang, G. Zhang, Photocatalytic degradation of organic contaminants by TiO_2/sepiolite composites prepared at low temperature, Chem. Eng. J. 173 (2011) 1–10.
[19] S. Yang, G. Liang, A. Gu, H. Mao, Synthesis of TiO_2 pillared montmorillonite with ordered interlayer mesoporous structure and high photocatalytic activity by an intra-gallery templating method, Mater. Res. Bull. 48 (2013) 3948–3954.
[20] Y. Jia, W. Han, G. Xiong, W. Yang, Layer-by-layer assembly of TiO_2 colloids onto diatomite to build hierarchical porous materials, J. Colloid Interface Sci. (2008) 326–331.
[21] K. Kočí, V. Matějka, P. Kovář, Z. Lacný, L. Obalová, Comparison of the pure TiO_2 and kaolinite/TiO_2 composite as catalyst for CO_2 photocatalytic reduction, Catal. Today 161 (2011) 105–109.

[22] C. Zhu, X. Wang, Q. Huang, L. Huang, J. Xie, C. Qing, T. Chen, Removal of gaseous carbon bisulfide using dielectric barrier discharge plasmas combined with TiO_2 coated attapulgite catalyst, Chem. Eng. J. 225 (2013) 567–573.
[23] Z. Korunic, Review Diatomaceous earths, a group of natural insecticides, J. Stored Prod. Res. 34 (1998) 87–97.
[24] M. Wang, Y. Xiang, G. Zhang, J. Song, D. Cai, Z. Wu, A facile approach to improve the quality of diatomite as sulfuric acid catalyst support, Appl. Catal. A: Gen. 466 (2013) 185–189.
[25] Z. Sun, X. Yang, G. Zhang, S. Zheng, R.L. Frost, A novel method for purification of low grade diatomite powders in centrifugal fields, Int. J. Miner. Process. 125 (2013) 18–26.
[26] Z. Sun, C. Bai, S. Zheng, X. Yang, R.L. Frost, A comparative study of different porous amorphous silica minerals supported TiO_2 catalysts, Appl. Catal. A: Gen. 458 (2013) 103–110.
[27] X. Liu, C. Yang, Y. Wang, Y. Guo, Y. Guo, G. Lu, Effect of the diatomite pretreatment on the catalytic performance of TS-1/diatomite for toluene hydroxylation by H_2O_2 in fixed-bed reactor, Chem. Eng. J. 243 (2014) 192–196.
[28] Y. Xia, F. Li, Y. Jiang, M. Xia, B. Xue, Y. Li, Interface actions between TiO_2 and porous diatomite on the structure and photocatalytic activity of TiO_2-diatomite, Appl. Surf. Sci. 303 (2014) 290–296.
[29] W. Xiao, J. Chen, K. Weng, W. Peng, G. Wang, F. Wang, High-temperature transformation of changbaishan diatomite and the formation mechanism of cristobalite, Acta Miner. Sin. 1 (2005) 20–26.
[30] S. Yamazaki, N. Fujinaga, K. Araki, Effect of sulfate ions for sol–gel synthesis of titania photocatalyst, Appl. Catal. A: Gen. 210 (2001) 97–102.
[31] Z. Zhang, C. Wang, R. Zakaria, J.Y. Ying, Role of particle size in nanocrystalline TiO_2-based photocatalysts, J. Phys. Chem. B 102 (1998) 10871–10878.
[32] S. Yi, P. Wu, Two-dimensional ATR-FTIR spectroscopic investigation on water diffusion in polypropylene film: water bending vibration, J. Phys. Chem. B 107 (2003) 4224–4226.
[33] F. Fresno, M.D. Hernández-Alonso, D. Tudela, J.M. Coronado, J. Soria, Photocatalytic degradation of toluene over doped and coupled (Ti, M)O_2 (M=Sn or Zr) nanocrystalline oxides: Influence of the heteroatom distribution on deactivation, Appl. Catal. B: Environ. 84 (2008) 598–606.
[34] G. Yang, Z. Yan, T. Xiao, B. Yang, Low-temperature synthesis of alkalis doped TiO_2 photocatalysts and their photocatalytic performance for degradation of methyl orange, J. Alloys Compd. 580 (2013) 15–22.
[35] Q. Chen, D. Jiang, W. Shi, D. Wu, Y. Xu, Visible-light-activated Ce–Si co-doped TiO_2 photocatalyst, Appl. Surf. Sci. 255 (2009) 7918–7924.
[36] J. Zhong, J. Li, F. Feng, Y. Lu, J. Zeng, W. Hu, Z. Tang, Improved photocatalytic performance of SiO_2–TiO_2 prepared with the assistance of SDBS, J. Mol. Catal. A: Chem. 357 (2012) 101–105.
[37] L. Youji, Z. Xiaoming, C. Wei, L. Leiyong, Z. Mengxiong, Q. Shidong, S. Shuguo, Photodecolorization of Rhodamine B on tungsten-doped TiO_2/activated carbon under visible-light irradiation, J. Hazard. Mater. 227–228 (2012) 25–33.
[38] D. Wang, L. Xiao, Q. Luo, X. Li, J. An, Y. Duan, Highly efficient visible light TiO_2 photocatalyst prepared by sol–gel method at temperatures lower than 300°C, J. Hazard. Mater. 192 (2011) 150–159.
[39] E. Vassileva, T. Stoychev, C. Daiev, K. Hadjiivanov, Chromium speciation analysis by solid-phase extraction on a high surface area TiO_2, Analyst 125 (2000) 693–698.
[40] M.A. Barakat, Adsorption behavior of copper and cyanide ions at TiO_2–solution interface, J. Colloid Interface Sci. 291 (2005) 345–352.
[41] T. Zhang, T. Oyama, A. Aoshima, H. Hidaka, J. Zhao, N. Serpone, Photooxidative N-demethylation of methylene blue in aqueous TiO_2 dispersions under UV irradiation, J. Photochem. Photobiol. A: Chem. 140 (2001) 163–172.
[42] J. Zolgharnein, M. Bagtash, N. Asanjarani, Hybrid central composite design approach for simultaneous optimization of removal of alizarin red S and indigo carmine dyes using cetyltrimethylammonium bromide-modified TiO_2 nanoparticles, J. Environ. Chem. Eng. 2 (2014) 988–1000.
[43] C. Zhan, F. Chen, J. Yang, D. Dai, X. Cao, M. Zhong, Visible light responsive sulfated rare earth doped TiO_2@fumed SiO_2 composites with mesoporosity: Enhanced photocatalytic activity for methyl orange degradation, J. Hazard. Mater. 267 (2014) 88–97.
[44] P. Yuan, D.Q. Wu, H.P. He, Z.Y. Lin, The hydroxyl species and acid sites on diatomite surface: a combined IR and Raman study, Appl. Surf. Sci. 227 (2004) 30–39.
[45] W. Baran, E. Adamek, A. Makowski, The influence of selected parameters on the photocatalytic degradation of azo-dyes in the presence of TiO_2 aqueous suspension, Chem. Eng. J. 145 (2008) 242–248.
[46] B. Cuiping, X. Xianfeng, G. Wenqi, F. Dexin, X. Mo, G. Zhongxue, X. Nian, Removal of rhodamine B by ozone-based advanced oxidation process, Desalination 278 (2011) 84–90.
[47] R. Jain, M. Mathur, S. Sikarwar, A. Mittal, Removal of the hazardous dye rhodamine B through photocatalytic and adsorption treatments, J. Environ. Manage. 85 (2007) 956–964.